Monthly Notices
of the
ROYAL ASTRONOMICAL SOCIETY

MNRAS **482,** 2407–2421 (2019)
Advance Access publication 2018 October 17

doi:10.1093/mnras/sty2772

Characteristics of organic matter on Ceres from VIR/Dawn high spatial resolution spectra

M. C. De Sanctis,[1]★ V. Vinogradoff,[1,3]★ A. Raponi,[1] E. Ammannito,[2] M. Ciarniello,[1] F. G. Carrozzo,[1] S. De Angelis,[1] C. A. Raymond[4] and C. T. Russell[5]

[1]*Istituto di Astrofisica e Planetologia Spaziali, INAF, 00133 Rome, Italy*
[2]*Agenzia Spaziale Italiana, 00133 Rome, Italy*
[3]*Aix-Marseille Université, PIIM UMR-CNRS 7345, F-13397 Marseille, France*
[4]*Jet Propulsion Laboratory, Pasadena, CA 91109, USA*
[5]*Institute of Geophysics and Planetary Physics, University of California, Los Angeles, CA 90095-1567, USA*

Accepted 2018 October 4. Received 2018 September 07; in original form 2018 May 21

ABSTRACT

Ceres is the largest object in the main belt and is a wet body with a complex geological and chemical history. Its surface is composed of opaque materials, phyllosilicates, ammoniated-bearing minerals, carbonates, water ice, and salts. Recently, aliphatic organics, whose origin is still uncertain, have also been detected on the Ceres surface by the imaging spectrometer Visible and Infrared Spectrometer (VIR) on board Dawn. Here, using VIR spectra, acquired with a high spatial resolution (< 100 m), we have analysed the organic-rich areas, their spectral characteristics, and the associated mineralogy. The new VIR spectra in the 3.2–3.6 μm spectral range have been compared to organic standard compounds measured in the laboratory, to investigate more deeply the nature of the organic matter on Ceres. The mineralogy appears quite complex, and the organic matter is often associated with a larger amount of ammoniated phases and carbonates. The detailed spectral analysis, as well as the laboratory comparison, reveal the presence of a band at 2.99–3 μm, likely associated with organic or inorganic NH-compounds (amine or salts), and the organic matter may be characterized by a rather low abundance of oxygen atoms. Spectral models of the organic material indicate that hundreds of meters-size areas can be very rich in aliphatic organics, with an estimated organic amount larger than the quantity normally found in CC meteorites. The mineralogical context and the retrieved amounts suggest that the aliphatic organic is likely a Ceres' endogenous product, and we formulate a hypothesis for the formation and evolution of the organic matter inside Ceres.

Key words: astrochemistry – techniques: imaging spectroscopy – minor planet: Ceres.

1 INTRODUCTION

Ceres is the largest object in the main belt and appears to be a wet body with a complex history (Russell et al. 2016). Ceres' surface is covered by opaque materials, phyllosilicates, ammoniated-bearing hydrated minerals, carbonates, and localized water ice and salts (De Sanctis et al. 2015; Combe et al. 2016; Carrozzo et al. 2018). The observed mineralogy and its distribution at the surface indicates a complex global evolution and a favourable environment for organic matter (De Sanctis et al. 2015; Ammannito et al. 2016; Russell et al. 2016). Spectra of Ceres acquired by the visible and infrared mapping spectrometer (VIR) on board the Dawn spacecraft (De Sanctis et al. 2011), are characterized by strong absorption features at 2.72, 3.05–3.1, and 3.96 μm. The most prominent is a strong and narrow absorption centred at 2.72–2.73 μm, due to OH-bearing phyllosilicates (Bishop et al. 2002). The comparison between the Ceres OH-band and those of terrestrial phyllosilicates indicates the presence of Mg-OH phases (De Sanctis et al. 2015, 2018; Ehlmann et al. 2018). The other features are attributed to carbonates (∼3.96 μm) and ammoniated phyllosilicates (∼3.06 μm). In addition, a strong signature between 3.3 and 3.6 μm has been observed near Ernutet (De Sanctis et al. 2017), a large crater at Lat ∼53°N, Lon ∼45.5°E. These features have been attributed to overlapping absorptions of carbonates and aliphatic carbons from organic matter (OM). The organic material is mainly localized in the Ernutet region (Fig. 1), but it has also been observed in a few other locations, such as Inamahari and Omonga craters. The aliphatic organic material has been observed as mixed with other minerals, which are ubiquitous on the Ceres surface, but some materials, such as NH_4-bearing minerals

★ E-mail: mariacristina.desanctis@inaf.it (MCDS);
vassilissa.vinogradoff@univ-amu.fr (VV)

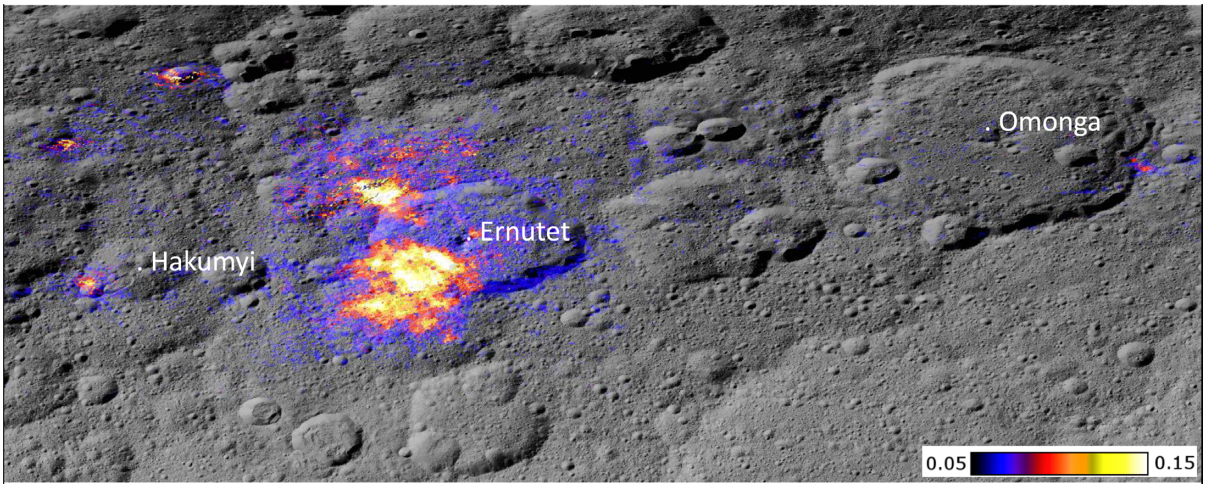

Figure 1. Geologic context of the Ernutet region on Ceres that exhibits organic material highlighted by the distribution of the 3.4-μm band depth. Band depths are calculated according to Ammannito et al. (2016) and cylindrically projected on framing camera (FC) clear filter mosaic. [FC mosaic photo credit: NASA/Jet Propulsion Laboratory – California Institute of Technology/University of California, Los Angeles/Max Planck Institute for Solar System Research/German Aerospace Center/Institut für Datentechnik und Kommunikationsnetze]

and/or carbonates, show an enhancement in the same region where organics were found (De Sanctis et al. 2017; Raponi et al. 2017).

To achieve a better understanding of the distribution, composition, and relation with the mineral phases of these organic-rich areas around the Ernutet crater, we have analysed VIR data taken at LAMO (Low Altitude Mapping Orbit) orbital phases, at a spatial resolution of less than 100 m. The resulting spectra of the OM in the 3.2–3.6 μm spectral range have been examined to derive some chemical properties by means of comparison with standard measurements by SPIM, the spare VIR spectrometer at the IAPS-INAF laboratory (De Angelis et al. 2015).

The origin, endogenous or exogenous, of the organic material on Ceres is still a matter of debate in the community (De Sanctis et al. 2017; Pieters et al. 2017), and these new data can help in discriminating among the different origins. Relying on the VIR LAMO data, we have tried to understand the mineralogy of the small areas with a high abundance of organic material and to estimate the amount of organic material modelling the spectra using Hapke's radiative transfer model (Hapke 2012). We discuss the origin and evolution of the OM in Ceres, based on the formation and evolution of organic matter in meteorites, as well as in hydrothermal vents.

2 METHOD

2.1 Data analysis

The spectra investigated in this work have been obtained with the VIR (De Sanctis et al. 2011). The high spatial (IFOV = 250 μrad/pixel, FOV = 64 × 64 mrad) and spectral ($\Delta\lambda_{VIS}$ = 1.8 nm/band; $\Delta\lambda_{IR}$ = 9.8 nm/band) resolution coupled with low-altitude orbits permitted the analysis of small surface features. Images are acquired using a scanning mirror or using the S/C movement with respect to the body surface: the scene is scanned one line at a time through the entrance slit of the spectrometer. Each line is made of 256 pixels. Thus, it is possible to extract a spectrum from each pixel of the image, showing the intensity of light as a function of the wavelength for that specific pixel. The data were calibrated and processed using the VIR calibration pipeline (Carrozzo et al. 2016). Both the flat field and the spectral response are improved in this calibration with respect to the previously published Vesta data (Carrozzo et al. 2016; De Sanctis et al. 2018). Ceres spectra are affected by thermal emission at the longest wavelengths of the investigated spectral range, and we implemented an algorithm to remove this contribution. This is done by modelling the total radiance as the sum of the solar radiance reflected by the surface and the thermal emission of the surface itself, and then performing the removal of the latter, as fully described in Raponi et al. (2017).

The investigated area is part of the mid-latitude Coniraya quadrangle (Ac-2) in the northern hemisphere of Ceres (Pasckert et al. 2017). Ernutet is a large complex crater (∼52 km in diameter; 53°N, 46°E) (Fig. 1) at the center of the quadrangle. Its age has been estimated to be ∼1.6 Ga (Lunar Derived Model), and the floor is relatively smooth, with several smaller and younger craters. The organic-rich areas are identified by the presence of a prominent 3.4-μm absorption band in the VIR spectra, also associated with the red-sloped visible colour in the Framing Camera images (Pieters et al. 2017).

Hereafter, we report on the analysis of the spectra obtained during the LAMO phase, at a resolution of about 100 m/pixel. The data cover only a small part of the region of interest, thus limiting the investigation to those specific areas, as indicated in Fig. 3. Despite the limited coverage, the good quality of the high-resolution observations permits a detailed examination of specific features, as detailed below.

2.2 Laboratory measurements

All the organic compounds measured were bought to Sigma–Aldrich and are represented by Polybutadiene (slabs, average Mw 200.000- [$CH_2CH = CHCH_2$]n), trans-Polyisoprene (pellets, 99 per cent—[$CH_2CH = C(CH_3)CH_2$]n), Paraformaldehyde (synonym polyoxymethylene, POM, powder—HO[CH_2O]nH), Poly (methyl methacrylate) (powder, PMMA– average Mw 15.000– [$CH_2C(CH_3)(CO_2CH_3)$]n), Poly-vinyl-methyl-ketone (slabs, PVMK—[$CH_2CH(COCH_3)$]n), Fluorene (98 per cent—$C_{13}H_{10}$). Asphaltite rock comes from an ancient mine at Mount Obachelle in the Italian Central Apennines, within the massif of Monte Cairo (Latium, Italy). We measured a portion of the fresh

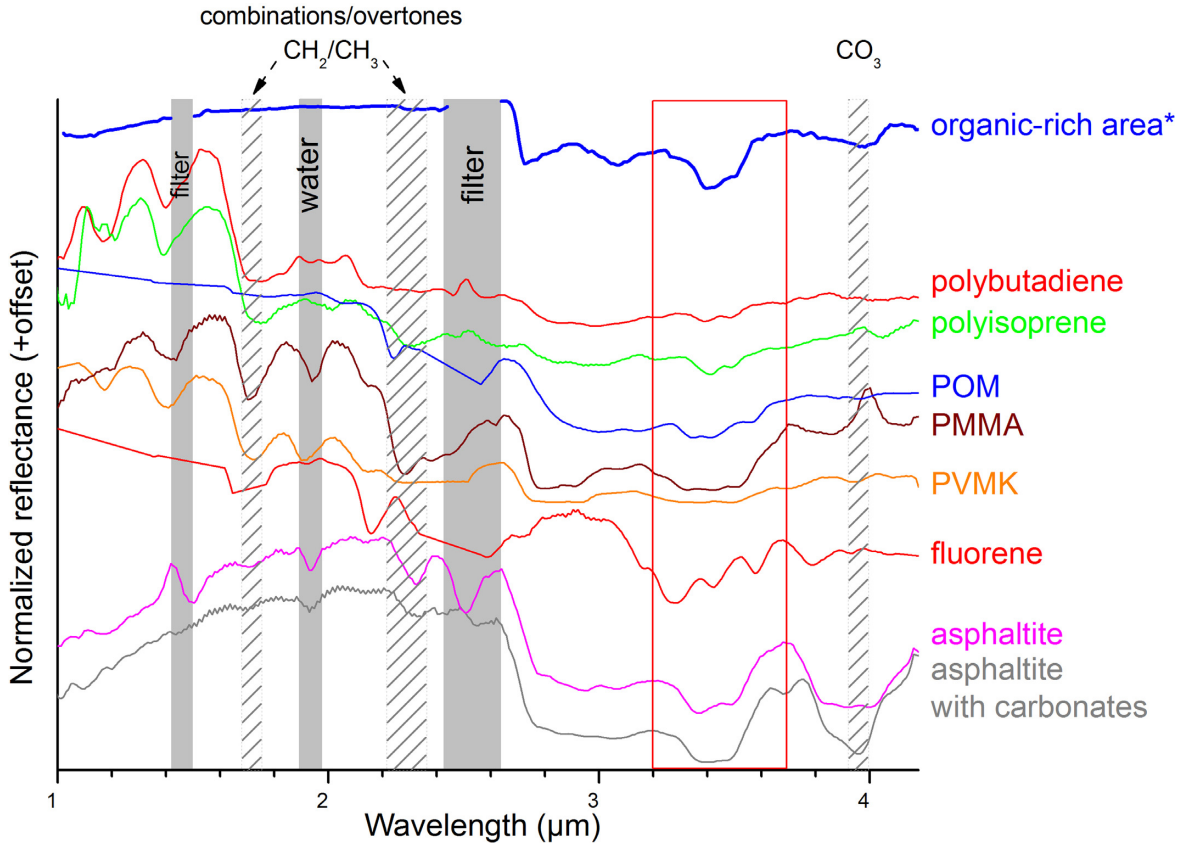

Figure 2. Infrared spectra of the standards measured with SPIM, presented in the 1–4.2 μm range. Laboratory spectra have been normalized and offset for clarity. Ceres spectrum (from De Sanctis et al. 2017) has been scaled (∗ x1.3) and offset for comparison. The vertical grey, full-pattern ribbons indicate the spectral range of filter and of absorbed water in the samples. The vertical grey ribbons with a hatched pattern indicate the spectral range of combinations and overtones of the CH_2 and CH_3 stretching bands, and of the CO_3 band of carbonates.

interior of the carbon layer (bitumen layer-slab), without any extraction. All samples were dried in a desiccator at 40°C for 4 h before analysis.

For comparison, we also used spectra of bitumen from RELAB (RELAB), one sample of oil shale (RELAB name: OS-EAC-014), and two samples of oil sand with different bitumen abundances (RELAB name TS-EAC-006-A: oil sand 1, 3.4 per cent bitumen and TS-EAC-010-A: oil sand 2, 9.1 per cent bitumen).

We have used the SPIM facility (all details on SPIM can be found in De Angelis et al. 2015) at IAPS-INAF to measure the organic samples in reflectance mode. SPIM is a laboratory spare of the VIR instrument on board the Dawn spacecraft, thus measurements done with SPIM can be easily compared with measurements done by VIR. It is an imaging spectrometer in the visible (VIS) and infrared (IR) spectral range 0.2–5.1 μm. The spatial resolution is 38 μm/pixel with a spectral resolution of 12 nm in the IR range. Labsphere Spectralon 99 per cent and Infragold were used as reference targets in order to retrieve reflectance spectra of the materials. All the samples have been measured at room temperature and pressure. Band shifts for the aliphatic features are not expected with temperature and pressure changes in the range interested. Fig. 2 shows a comparison between Ceres organic-rich spectrum and the measured samples.

3 VIR DATA

The distribution of organic material in the large Ernutet region was mapped using the band depth at 3.4 μm as a proxy of the organic content (De Sanctis et al. 2017; Raponi et al. 2017, Fig. 1).

In Ernutet, the organic material is found mainly in two broad areas: one is a roughly triangular region in the northwestern portion of the crater (A in Fig. 3), and one is located on the southwestern part (B in Fig. 3). In both cases, organic material is found inside and outside the crater, concentrated in small areas as well as in diffuse regions between the two main concentrations (De Sanctis et al. 2017; Raponi et al. 2017). Moreover, several other small discrete or diffuse areas are found several tens of kilometers both west and east of Ernutet. An interesting concentration of OM, (C in Fig. 3) is found in a small fresh 6.5-km crater and lobate flow, located ∼70 km to the west of Ernutet on the rim of the Hakumyi crater (29 km in diameter; ∼51N°, 28°E, Fig. 1). To highlight the difference of these spots with respect to the surroundings, we computed the spectral ratio of the specific spectra with the background spectra (Fig. 4). The background spectra are taken from a region far from the organic-rich spot, but observed by the same pixels of the detector to avoid, as much as possible, instrumental effects.

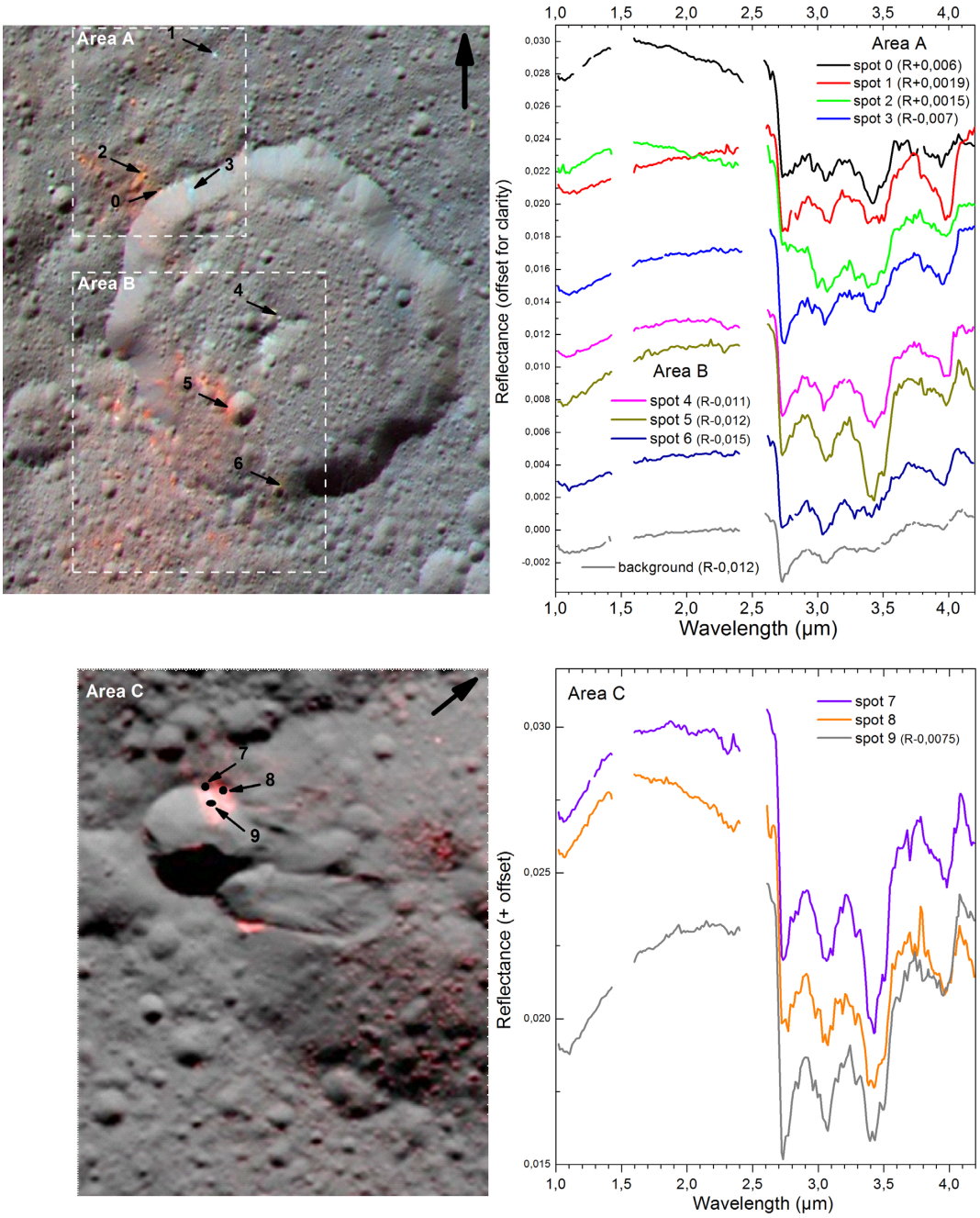

Figure 3. (Left) Enhanced Framing Camera (FC) colour images of the Ernutet area (top) and Hakumyi area (bottom), illustrating the context regions of the spectra analysed here (adapted from Pieters et al. 2017). Reddish colours in these images correspond to a high concentration of organics. Spots numbered from 0 to 9 correspond to local organic-rich concentrations or carbonate-rich concentrations, based on the 3.4 and 3.9 μm band depth. (Right) VIR spectra of the corresponding local concentrations (spots) numbered on the figures on the left. The spectrum of a typical background is also shown for reference. The black arrow indicates the north on the images and the *R–X* in the plots indicates an offset of reflectance for clarity.

3.1 Area A

This region extends from the crater floor to outside of the crater rim, with the presence of organic material (OM) in small localized areas (as in spot 0 of Fig. 3). This region is also characterized by band depths stronger than the average of 3.4 μm. The area shows a different concentration in the mineral phases, carbonates and ammoniated-phyllosilicates. For example, spot 1 is characterized by a relatively large content of carbonates with respect to other spots (Fig. 3).

All the observed spectral ratio of the spots show an intense band at 3.4 micron and a peak at about 2.7 micron, the latter corresponding to the wavelength of the phyllosilicate OH band. The peak may suggest fewer phyllosilicates in the analysed spots with respect to the background.

The enhanced band at 3.4 μm cannot be justified by the presence of only additional carbonates with respect to the background. The spectra of the spots in Fig. 3 show an intense 3.4 μm band, which, in most cases, are stronger than the 3.96–4 μm bands. As shown in

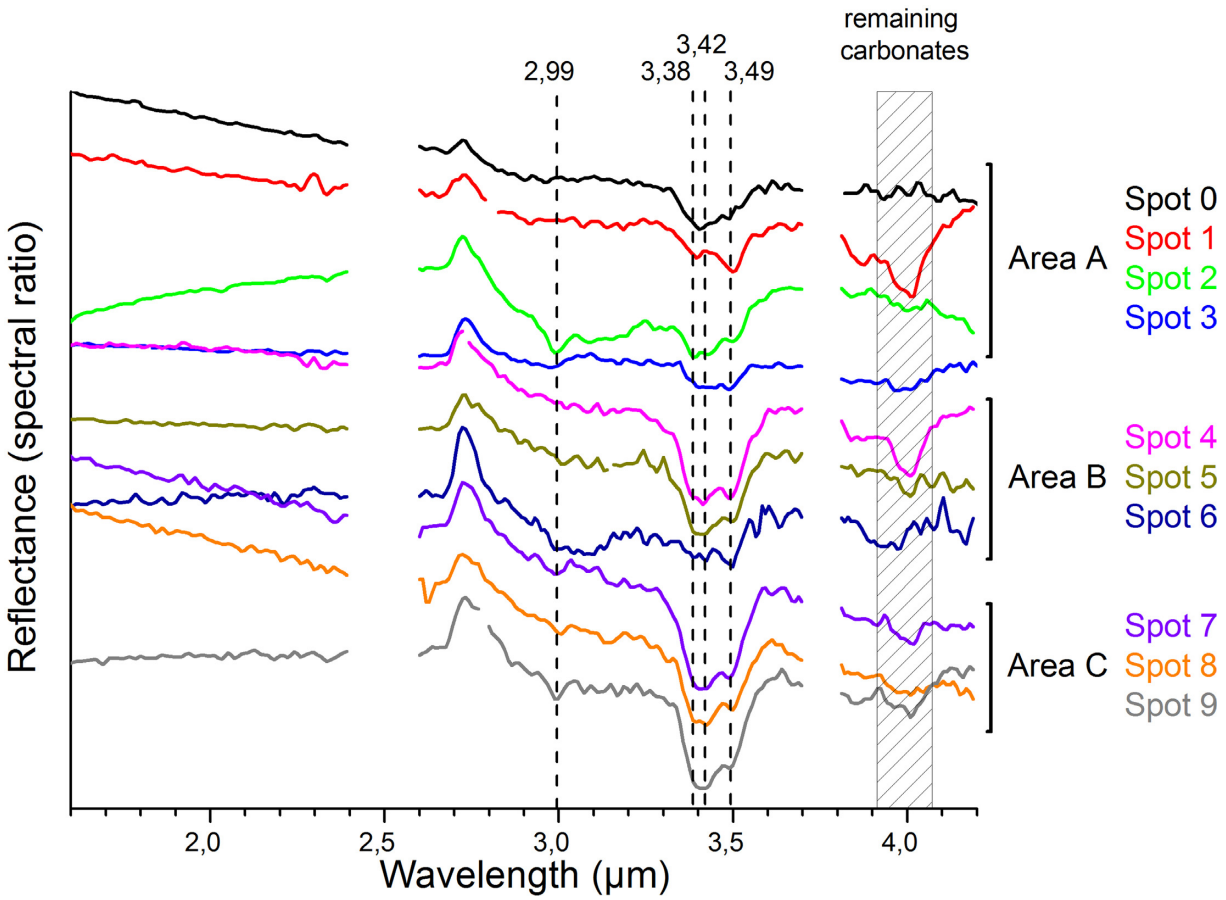

Figure 4. Spectral ratio of the spectra in Fig. 3. Spectral ratios have been computed using spectra of background material. The vertical lines highlight specific wavelengths. The dashed rectangular box indicates the spectral region where signatures of carbonates are visible.

Fig. 3, the comparison between the spectra of spot 0 and 1 shows how much the band at 3.4 μm is different in the two cases. In case of predominantly carbonates (spot 1), the band at 3.4 μm is less pronounced with respect to the 3.96–4 μm band, while in the case of mainly organics (spot 0), the 3.4-μm band is more pronounced with respect to the 3.96–4 μm band. Moreover, the shape of the 3.4 μm band in the two cases is diverse. The differences can be also seen in the spectral ratio shown in Fig. 4, where no carbonate band is apparent in spot 0, while no organic band is apparent in spot 1. Other spots may have a small extra amount of carbonate with respect to the background, but not an amount sufficient to justify the shape and depth of the 3.4 μm band, as also demonstrated by the spectral fitting analysis (Sec. 5.3).

Spot 0, on Ernutet's crater rim, shows a strong band at 3.4 μm that is typical for this organic-rich area. The remaining absorptions at 2.72, 3.06, and 3.96 μm in the spectrum are similar to those in the background spectra, as demonstrated by the spectral ratio between spot 0 and the background (Figs. 4 and 5).

The very small crater in spot 1 presents a strong signature of carbonates at about 3.96–4.0 μm. The minimum of the carbonate band shows a clear shift towards longer wavelengths with respect to the background area, that has a smaller carbonate band at about 3.96 μm. A similar shift has been observed in several areas of Ceres (Carrozzo et al. 2018), notably in Occator (De Sanctis et al. 2016; Raponi et al. 2018), where it has been interpreted as due to the presence of natrite, a sodium carbonate (Na_2CO_3). The comparison between the spectrum of natrite and the spectral ratio of spot 1 with background material (Fig. 5) clearly shows the presence of natrite in this small area.

Another interesting area is found in a small crater (indicated as spot 2 in Fig. 3), in the northern ejecta of Ernutet. This small area shows a spectrum different from even the previous one discussed (Fig. 6).

The spectrum of spot 2 shows a complex and deep band extending from 2.6 to 3.8 μm. Several differences arise from the comparison between the background and spot 2 (Fig. 6). The phyllosilicate OH band minimum at 2.7 μm is flatter and shows a shift of the band minima towards longer wavelengths. The band at 3.07 μm, commonly associated with ammoniated phyllosilicates, is very strong and shows a clear additional minimum centred at 2.99–3.0 μm. This area shows also a prominent band at 3.4–3.6 μm, which can be associated with aliphatic organics.

3.2 Area B

Area B, on the floor of the crater and encompassing the south rim of Ernutet, shows several small concentrations of organic material. Among them here we examine: spot 4, on the Ernutet central peak; spot 5, on the wall and rim of a crater on the Ernutet floor; and spot 6, a small crater on the south rim of Ernutet (see Fig. 2). The spectrum taken from a small area on the central peak of Ernutet (spot 4) not only shows a strong organic band but also a strong carbonate band with a flat minimum, possibly associated with the presence of Mg, Ca-carbonate and Na-carbonate.

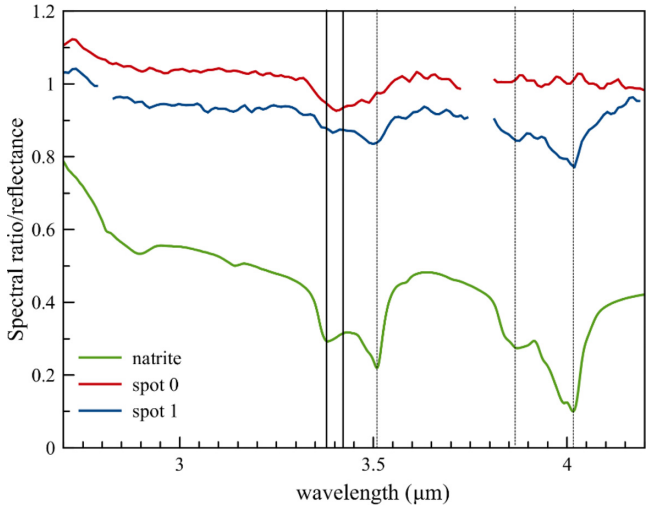

Figure 5. Spectral ratio of spot 0 and 1 with background in comparison to a laboratory spectrum of natrite CB-EAC-034-C, RELAB). Vertical dotted lines highlight the carbonate absorption minima, and solid vertical lines indicate CH2 (3.42 μm) and CH3 (3.38 μm) main absorptions. The line at 3.42 μm corresponds also to a carbonate absorption.

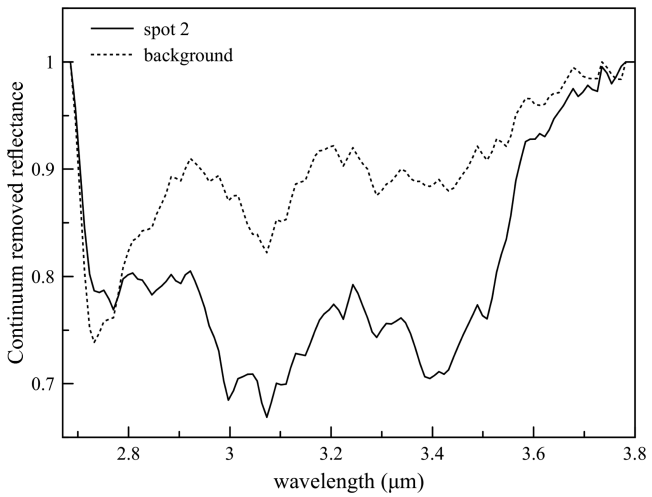

Figure 6. Continuum-removed spectra of spot 2 (black line) and background material (dashed line). The continuum has been removed with a straight line between 2.66 and 4.1 μm.

The spectrum extracted from a few pixels in spot 5, on the rim of the crater on Ernutet floor, shows a strong 3.4-μm band and a broad and deep absorption at 3.07 μm. It is also characterized by a shift of the 3.96–4 μm carbonate band towards longer wavelengths with respect to the background. The spectrum of the small crater on the rim of Ernutet, spot 6, has almost no absorption at 3.4 μm but has a broad band at 3.07 μm.

The spectra of these small areas have been ratioed by spectra of the background, in order to highlight the main differences with respect to the crater floor and ejecta (Fig. 3). We can clearly observe the presence of carbonates in spot 4 with the band at 4.01 μm, which is also found in spot 5 but is less pronounced, interpreted as Na-carbonates (De Sanctis et al., 2016, 2018; Carozzo et al. 2018). The ratioed spectrum of spot 6 is noisier due to the unfavorable illumination conditions when the data were acquired. Nevertheless, bands at 3.4 μm and 3.95 μm can be seen in the spectrum with an additional broad absorption between 3 μm and 3.2 μm.

3.3 Area C (in Hakumyi crater)

Hakumyi crater is located ~70 km to the west of Ernutet. A smaller crater (6.5 km in diameter) occurred on Hakumyi, potentially associated with the emplacement of a lobate flow deposit (Fig. 3). Both the crater rim and the lobate flow have a signature of organics, identified by the VIR High-Altitude Mapping Orbit (HAMO) data (De Sanctis et al. 2017). Unfortunately, LAMO data of the lobate flow are not available, thus the investigation is only limited to the crater rim. The material on the rim of this fresh crater (50.5N°/25.5°E) exhibits a strong organic band, as shown in the spectra of Fig. 4, all associated with strong absorptions at 3.95 μm and 3.07 μm of carbonates and ammoniated-phyllosilicates, respectively. Compared to the background, the three spectra (spots 7, 8. and 9) present a very strong and fairly similar 3.4-μm band, with a minor contribution of carbonates at 4.01 μm, again suggesting the presence of Na-carbonates. The three spectral ratios also indicate the presence of a small band at 2.99–3 μm (Fig. 4), such as the one observed in spot 2 of area A.

4 LABORATORY MEASUREMENTS OF ORGANIC SAMPLES AND COMPARISON WITH VIR DATA

In order to obtain more information on the nature of the OM observed in the three different areas around Ernutet, we have compared four of the more different spectra extracted from the VIR LAMO data with polymers, polycyclic aromatic compounds (PAHs) measured in reflectance in the laboratory (Figs 2,7) and organic-rich shales (see methods).

Polybutadiene and polyisoprene polymers display well-defined bands at 3.40 and 3.41 μm, respectively, which correspond to $\nu_{as}(CH_2)$ methylene groups, and one band centred at 3.48 μm attributed to $\nu_s(CH_2)$ groups (Coates 2006). The additional methyl group in the polyisoprene is observed with the shoulder at 3.37 μm, corresponding to $\nu_{as}(CH_3)$ that modifies the shape of the $\nu_{as}(CH_{2/3})$ band. Compared to VIR spectra, the $\nu_{as}(CH_2)$ band is shifted towards shorter wavelengths, likely due to alkene groups in the polymer (Coates 2006).

The presence of oxygen functions OH/C = O has a clear impact on the 3.2–3.7 μm shape, as attested with the POM, PMMA, and PVKM polymers. The whole band is broader with a shift of the $\nu_{as}(CH_3)$ contribution for the PMMA and PVKM polymers towards shorter wavelengths due to the influence of the ester or ketone function (both at 3.34 μm), which is not observed in the VIR spectra. The stretching $\nu_s(CH_{2/3})$ band is also slightly shifted, especially for the PMMA polymer at 3.52 μm. Additionally, the POM has a broad and intense absorption between 2.6 and 3.2 μm, corresponding to the alcohol functions at the end of the chains (Schutte, Allamandola & Sandford 1993). No alcohol or carboxylic acid bands are clearly observed in the VIR spectra. To note, the POM has a contribution at 3.34 μm due to combination and overtone modes and a band at 3.56 μm which corresponds to a Fermi resonance (Schutte, Allamandola & Sandford 1993; Danger et al. 2014). PVMK and PMMA have water contribution at 2.8–3 μm because they are hygroscopic compounds and we were not able to remove the water for the measurements.

The IR spectra of aromatic compounds, such as fluorene, feature

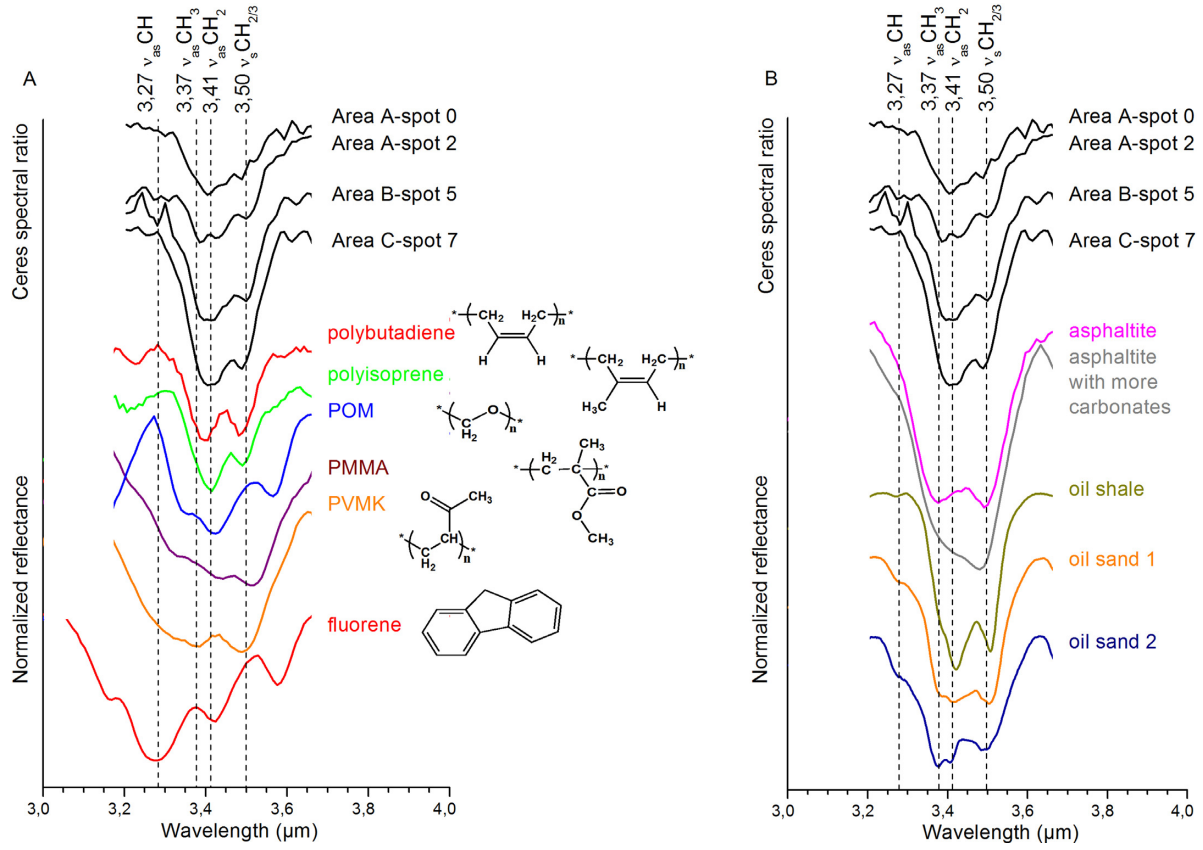

Figure 7. Infrared spectra of some of Ceres' spots described before compared to infrared spectra of A) polymers and organic compounds, and B) asphaltite, oil shale, and oil sand. Peak positions and assignment from Coates (2006).

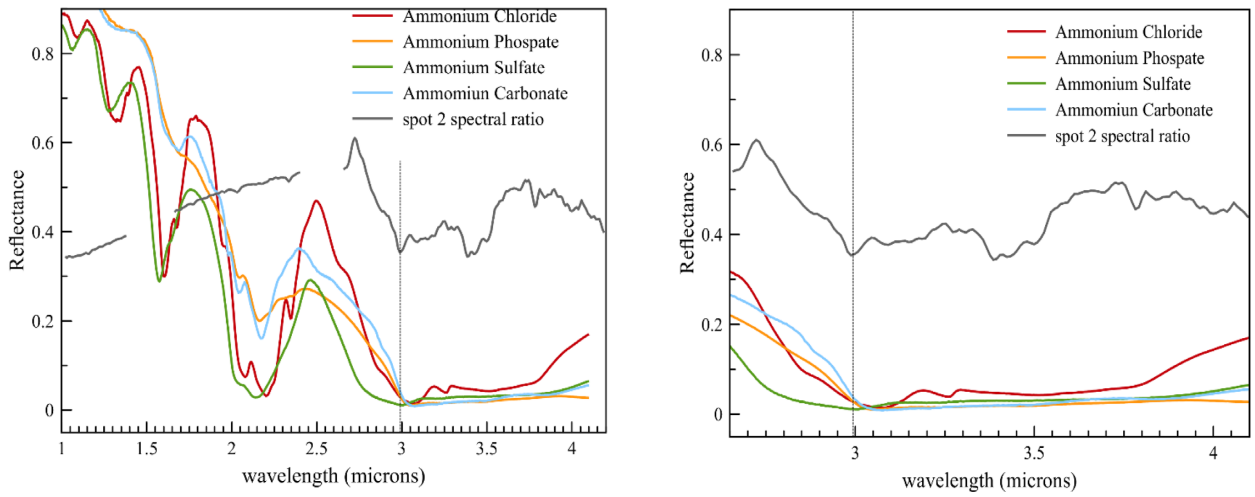

Figure 8. Laboratory spectra of ammonium salts (RELAB) in comparison with spot 2 spectral ratio. The spectral ratio has been offset for clarity.

a clear absorption at 3.27 μm, corresponding to the ν_{as}(CH) band of aromatic carbons (Bree & Zwarich 1969), which is not observed in the VIR spectra. Additional peaks are observed on the fluorene spectrum, at 3.42 μm, corresponding to the absorption of the methylene group and at 3.6 μm and 3.16 μm, which are probably issued from a Fermi resonance or an overtone.

Terrestrial oil shale and oil sand are good terrestrial analogues because they are composed of bitumen, an immature hydrocarbon made of soluble and insoluble compounds (Curiale 1986; Moroz et al. 1998; Bernard et al. 2012) (i.e., rich in aliphatic carbons with a disordered structure), containing a low abundance of heteroatoms (less than 10 wt per cent) (Curiale 1986; Moroz et al. 1998). Spectra

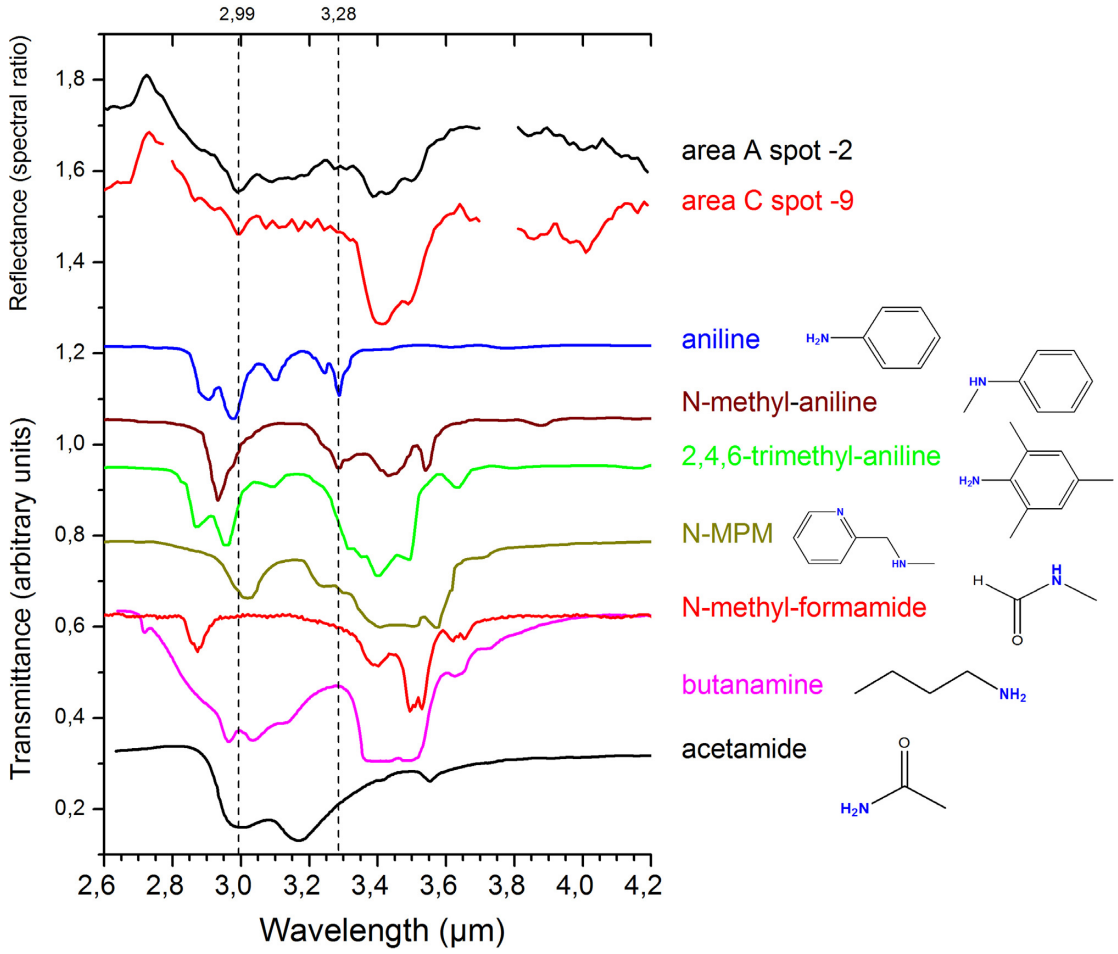

Figure 9. Comparison of the ratio of spot 2 and spot 9 with different amine spectra from the NIST database (Linstrom and Mallard 2018), to observe the variation of the NH stretching band position. N-MPM: N-methyl-2-pyrydylmethylamine. Butanamine spectrum is saturated in the 3.4 μm range, and does not display the features correctly. We emphasize that the amine spectra are in transmission mode and are displayed only for reference.

of this kind of material typically contain aliphatic features, with a variation of the CH (aromatic carbons), CH_2, and CH_3 stretching band intensities, as observed on the three spectra of different oils (from RELAB). Oil sand 2, which contains a higher abundance of bitumen than oil sand 1 (9.1 per cent instead of 3.4 per cent—see methods), displays a higher $\nu_{as}(CH_3)$ band. The band positions are perfectly consistent with the stretching mode of $\nu_{as}CH_2$ and $\nu_{as}CH_3$ modes (no shift) and fit nicely with the VIR data (especially oil sand 1).

5 INTERPRETATION

5.1 The 2.99 μm band

The investigation of the data at high spatial resolution permits the evaluation of the small-scale (at ∼100 m spatial resolution) mineralogy of this area, better constraining the nature of the organic material on Ceres. As reported before, the OM is found in small areas, where it is particularly abundant, and admixed, in lower proportion, with the average terrains. From the analysis of the rich OM spots emerges a complex mineralogy in terms of combination of organic material with other minerals. Most of these minerals have been identified on Ceres (NH_4-phyllosilicates and Mg-phyllosilicates, Na-carbonates, Mg, Ca-carbonates) and interpreted as the result of aqueous alteration and hydrothermal processes.

However, there are small organic-material-rich areas showing not only additional absorption bands, in particular spot 2, but also the spots in area C, described above. These regions show a strong absorption at around 3.1 μm (Fig. 3), indicating a high abundance of ammoniated-phyllosilicate. The spectral ratio highlights an absorption at about 2.99–3 μm (Fig. 4). This band is particularly evident in spot 2, along with the broad feature at 3–3.2 μm (Fig. 4).

The presence of this new feature in these areas can indicate the presence of other ammonium-bearing materials, like salts, and not only of that of ammoniated phyllosilicates, as in typical Ceres material. Most of Ceres' surface indeed shows a feature centered at 3.07 μm, interpreted as due to ammoniated phyllosilicates (King et al. 1992; De Sanctis et al. 2015). Additionally, salts of NH_4, such as NH_4Cl (ammonium chloride) have also been identified in Cerealia facula (the central bright dome in the Occator crater [De Sanctis et al. 2016; Raponi et al. 2018]).

Reflectance spectra of ammonium chloride, as well as ammonium sulfate, carbonate, and phosphate, do not show bands at 2.99 μm but are characterized by a strong absorption longward of 2.5 μm as well as strong and well-defined absorptions around 2.2 and 1.6 μm (see Fig. 8). These bands are not clearly discernible in the spectra of spot 2, but they are present in other Ceres areas, such as in Occator

Table 1. Spectra used in the fitting procedure. Sample name is indicated for reflectance spectra available on Relab database.

End-member	Sample name	Reference
Magnetite	MG-EAC-002	E.A. Cloutis, RELAB Spectral Library
Carbon		Zubko et al. 1996
Heated Natrite	CB-EAC-034-C	E.A. Cloutis, RELAB Spectral Library
Kerite_1	MA-ATB-043	A.T. Basilevsky, RELAB Spectral Library
Kerite_2		Moroz et al. 1998
High kerite/low antraxolithe		Moroz et al. 1998
Asphalitite		Moroz et al. 1998
Shocked Asphaltite	AS-LXM-004	L. Moroz, RELAB Spectral Library
Antigorite	AT-TXH-006	T.X. Hiroi, RELAB Spectral Library
NH_4-montmorillonite	JB-JLB-189	J. L. Bishop, SETI Institute
NH_4-annite	AA-A1S-002	A. Smirnov, State University of New York, Dept. of Geosciences
Dolomite	CB-EAC-003	E.A. Cloutis, RELAB Spectral Library
Ammonium Chloride	CL-EAC-049-A	E.A. Cloutis, RELAB Spectral Library
Ammonium Bicarbonate	CB-EAC-041-B	E.A. Cloutis, RELAB Spectral Library

bright material (De Sanctis et al. 2016; Raponi et al. 2018). Thus, the presence of a large amount of these kinds of salts to explain the 2.99 μm band is unlikely. Also, the spectral modelling of spot 2, including these salts, does not result in good fits (Fig. 8).

Other functional groups that have bands in the 3 μm range are OH- and NH-bearing organic compounds and can contribute to the absorption observed. Alcohol and carboxylic acids typically exhibit a broad-band between 2.6 and 3.2 μm, which is not compatible with the shape of the band at 2.99 μm, observed here (Coates 2006). Amine functional groups, NH_2- and NH-, however, show relatively well-defined absorptions in the range between 2.85 and 3.2 μm, typical of the asymmetrical and symmetrical NH stretching modes. The shape of these bands is characteristic of each specific compound with the general rule that primary amines (R-NH2) display two or three bands while secondary amines (R2-NH) display only one between 2.9 and 3.2 μm (Fig. 9).

The comparison of the spectral ratio of spot 2 and spot 9 with some amine spectra shows some similarities. In particular, amine functional groups linked to an aromatic ring seem to display a sharper NH stretching band than on the aliphatic chain, and the band depth of the CH and NH stretching modes are relatively similar. Moreover, the CH stretching mode of aromatic carbon can be erased by additional methyl substitution on the aromatic ring (see, for example, aniline and 2.4.6-trimethylaniline compounds spectra). Nonetheless, the peak position of the NH-stretching band largely varies with the structure and its environment, i.e., next to an aromatic ring, in an aliphatic chain, or next to an oxygen group.

The identification of the additional peak at 2.99 μm remains uncertain, but it is possible that the 2.99 μm spectral features are associated with the N–H bond, either as new ammoniated-mineral or organic amine compounds.

5.2 Insight on the nature of the OM from laboratory comparison

The identification of the organic material observed in Ceres is particularly challenging due to the limited spectral range and the overlapping of functional groups from organic and inorganic compounds. In particular, the C–H band of aromatic carbons (near 3.27 μm) is not clearly observed in Ceres OM spectra, but the lack of this band cannot exclude the presence of aromatic carbons. The C–H stretching band might be indeed difficult to observe due to a very low absorption cross-section (Dartois et al. 2007), but also because aromatic carbons might exist without having a hydrogen bond (i.e., without a C–H stretching band). The IR spectra of chondritic IOM (Orthous-Daunay et al. 2013) as well as of several organic-rich shales (Cloutis 2003; Lis et al. 2005), do not display the C–H stretching band, whereas the carbon in these OMs is involved for at least half of its abundance in aromatic compounds (Dela Rosa et al. 1992; Cody, Alexander & Tera 2002; Cody & Alexander 2005; Bernard et al. 2012). On the contrary, mature terrestrial organic matter, such as coals or kerogens, have strong absorption features at 3.27 μm, reflecting a high abundance of aromatic compounds with 'free' C–H aromatic bonds (Moroz et al. 1998; Cloutis 2003). For the IOM in carbonaceous chondrites (CC), it has been suggested that the carbon aromatic rings might contain abundant methyl and aliphatic chains or alcohol groups attached to the aromatic ring, resulting in a low abundance of free C–H aromatic bonds (Cody, Alexander & Tera 2002), while mature terrestrial matter contains less cross-linking. Hence, the non-observation of the CH aromatic stretching band in Ceres spectra do not exclude the presence of aromatic compounds in Ceres OM but instead can give some clues to the cross-linking level of the carbon structure. We have also noted for all the Ceres spectra that the CH_2 and CH_3 aliphatic bands of the antisymmetric stretching modes (3.41 and 3.37 μm, respectively), have almost equal intensity, and do not fit with a polymer containing only CH_2 carbons (such as polyisopene). This may indicate a high abundance of CH_3 groups in the OM of Ceres.

The shape of the spectral band between 3.2 and 3.6 μm and the well-defined band shape of the Ceres spectra seem to indicate the occurrence of mainly C–H atoms. A high abundance of OH groups, from alcohols or carboxylic acids, is not possible since these chemical compounds usually display a broad-band between 2.7 and 3.2 μm not observed in Ceres spectra. Carboxylic acid and/or alcohol compounds were proposed as plausible carriers of the 3.2 μm band observed in the VIRTIS spectra of the 67P/Churyumov–Gerasimenko comet (Capaccioni et al. 2015; Quirico et al. 2016), but these spectra are very different compared to those obtained from VIR. Nonetheless, oxygen molecules with ketone, aldehyde, esters,

Table 2. Retrieved abundances.

	Kerite_1 (%)	Antigorite (%)	NH_4-annite (%)	NH_4-montmor. (%)	Dolomite (%)	Natrite (%)	Magnetite (%)	Grain size (μm)
Spot 0	3.5	3.5	0	6	2.5	0	84.5	300
Spot 1	0	1	0	6	3	20	70	115
Spot 2	1	0	10	7.5	2.5	4.5	74.5	290
Spot 3	1	2.5	0	5.5	3	0	88	140
Spot 4	6	2.5	1.5	5.5	2.5	8	74	225
Spot 5	8.5	2.5	3.5	5.5	2	3	75	140
Spot 6	0.5	0	0.5	6.5	2.5	0	90	230
Spot 7	6.5	2.5	2	6	2	2	79	160
Spot 8	4.5	1.5	0	6	2	2	84	240
Spot 9	4.5	2.5	1	6	2	2	82	180

or ether functions might compose the Ceres OM. The IR spectra of oxygen-bearing compounds (such as PMMA, POM, and PVMK) show that a high abundance of oxygen functions (as ketone, ether) induces a shift of the band positions of $\nu_s(CH_{2/3})$ and $\nu_{as}(CH_{2/3})$ and an overall increase of the 3.2–3.6 μm band broadness. The width of the 3.2–3.6 μm Ceres band is limited and closer to one of insoluble organic matter (IOM) (De Sanctis et al. 2017) and organic-rich shales (this study). The IOM and the organic-rich shales are composed on average of an oxygen abundance at a maxima of 30 per cent wt (Dela Rosa et al. 1992; Cloutis 2003; Alexander et al. 2007). Based on the shape of the 3.2–3.6 μm CH aliphatic band in Ceres spectra and on the position of the stretching CH bands (no shift compared to theoretical values), we propose that the oxygen abundance in Ceres OM is not higher than 20–30 wt per cent and that the organic oxygen is involved mainly in ketone, ester, ether, or aldehyde functions.

Of note, we are unable to conclude from the data on the soluble or insoluble nature of this material at the surface of Ceres, as well as the exact composition of the OM. These remaining open questions can be addressed by seeking the history of the Ceres OM.

5.3 Spectral fit analysis

The spectra of the different spots studied here show several small differences that can reflect differences in composition and abundance of the different materials. To understand such differences, we have modelled the spectra of the areas described previously using Hapke's radiative transfer model (Hapke 2012) as described by Ciarniello et al. (2011) and Raponi et al. (2017, 2018). We choose to model the organic–rich spectra as an intimate mixture of the different spectral end-members, as listed in Table 1. We have modelled intimate mixing modalities in which the particles of the end-member materials are in contact with each other. The modelled reflectance is a function of the effective single scattering albedo which is obtained by a linear combination of the single scattering albedo of the different end members (Table 1).

The choice of the end members for the spectral fitting is primarily based on previous modelling of the average Ceres surface (De Sanctis et al., 2015, 2018) and of the bright material occurring on specific areas (De Sanctis et al. 2016; Carrozzo et al. 2018). For the organic component, we considered the same end members used for the previous fitting of the Ernutet area (De Sanctis et al. 2017; Raponi et al. 2017) along with additional compounds. Here, we include two bitumen of different composition to address the effect of decreasing H/C and O/C ratios and increasing aromaticity, taken from Moroz et al. (1998).

We also estimated the effects of the grain size of the organic end members in the abundances retrieved from the fitting procedure, as well as the effects of the type of opaque phase. The details of the method are given in Raponi et al. (2017, 2018). The material abundances retrieved from the fits are summarized in Table 2.

As baseline, in these fits, we assumed the same end-members used in De Sanctis et al. (2017), obtaining consistent results in terms of abundance of organic materials (Table 2). However, the results of the fitting procedure are not all equally satisfactory (Fig. 10). While the fitting model is able to reproduce most of them, the fits of spectra of spots 2 and 6 are not adequate, in particular, in reproducing the 3.07-μm band. The spectrum of spot 2 seems to require different materials as end-members for the fitting procedure. In this respect, we tried to include NH_4Cl and/or NH_4 HCO_3 as end-members, but the results are still unsatisfactory (Fig. 11).

Generally, we note that the band at 3.07 μm is not always fitted properly, with the observed organic-rich spectra showing a stronger band with respect to the fitting results. This general behavior could indicate that the organic-rich materials are also rich in ammoniated phyllosilicates or other ammonium compounds not yet identified. However, there are few laboratory spectra of ammoniated phyllosilicates (Bishop et al. 2002; Ehlmann et al. 2018) and the uncertainties on the fitting 3.07 μm band could be due to the limited spectra available for the fitting.

The retrieved abundances depend on the spectral end members used in the fitting procedure.

Here, for sake of simplicity, we used only one type of aliphatic organic (kerite_1) to fit the all spectra in Fig. 10, but we have demonstrated that the amount of organic material can largely vary as a function of the end-members used (De Sanctis et al. 2017). For instance, considering another spectrum of kerite (kerite_2, from Moroz et al. 1998), the abundance of organics obtained in spot 5 is slightly less (6.5 per cent) than the abundance derived using kerite_1.

Other types of aliphatic material with less pronounced bands at 3.4 μm, indicating a larger degree of aromaticity (Moroz et al. 1998), can give a larger abundance of organic material, as in the case of high kerite/low antraxolithe (from Moroz et al. 1998). However, if we use this end-member to fit spot 5, the estimated amount of organics is about 9.5 per cent, but the fit is unsatisfactory, with a pronounced aromatic band not visible in the spectra of spot 5 (Fig. 12a). This result indicates that an organic component with an intermediate degree of aromaticity is not suitable to reproduce the spectra studied here. Considering as end member a shocked asphaltite (AS-LXM-004, RELAB) to fit the spectrum of spot 5, the estimated abundance is much larger (25 per cent) (Fig. 12b).

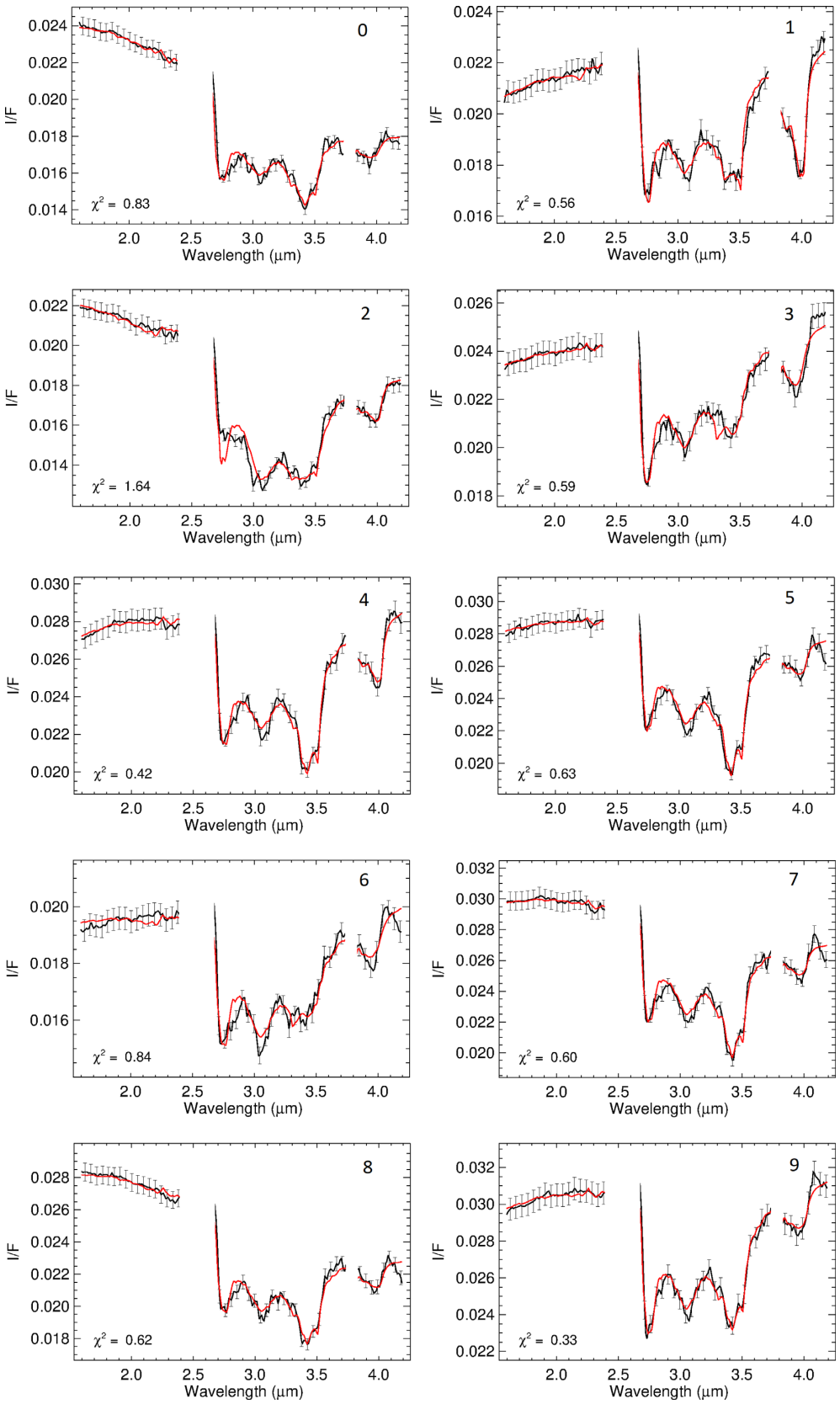

Figure 10. Spectral fits of the areas identified in Fig. 3, using the end members described in Table 1. The end member used to represent the organic component is kerite_1 (Table 1. *Y*-axis: radiance factor (π x reflectance) after thermal removal, hereafter called I/F. Black lines: measured spectra with error bars estimated from calibration uncertainties (Carrozzo et al. 2016). Red lines: modelled spectrum.

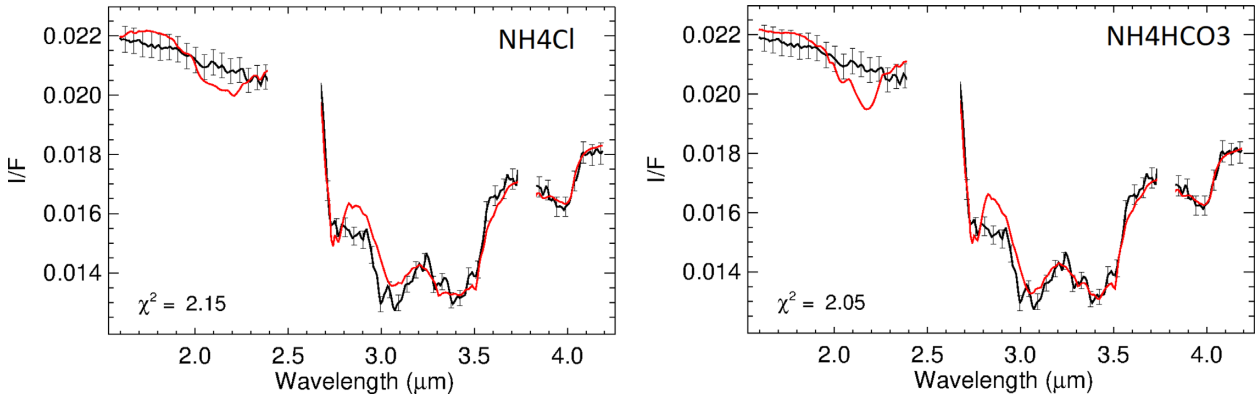

Figure 11. Spectral fits of spot 2, including the presence of NH_4Cl or NH_4HCO_3 (Table 1 for reference). Black lines: measured spectra with error bars estimated from calibration uncertainties (Carrozzo et al. 2016). Red lines: modelled spectrum.

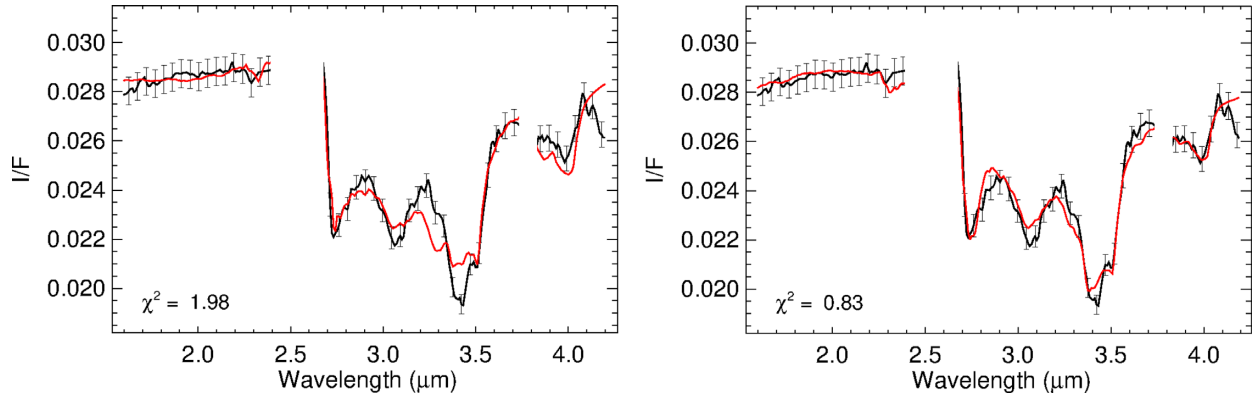

Figure 12. (Left) Spectral fit of spot 5 using high kerite/low antraxolithe spectrum as the end member for the organic component. (Right) Spectral fit of spot 5 using shocked asphaltite spectrum as the end-member for the organic component. Black lines: measured spectra with error bars estimated from calibration uncertainties (Carrozzo et al. 2016). Red lines: modelled spectrumthis.

Along with the selection of the end members, their grain size can also affect the derived abundances. For example, we fit spot 5 using the spectra of asphaltite (Moroz et al. 1998) at different grain size, from < 25 μm to 125 μm. The retrieved abundances show slight differences ranging from 4 per cent to 5 per cent (see Table 3).

Another factor influencing the retrieved abundances is the type of opaque material used in the fit, as can be seen by the results of the modelling, considering magnetite or carbon as dark material. As a general trend, we see that considering carbon as an opaque phase, the estimated amount of organics is about 1–2 per cent less with respect to the usage of magnetite (Table 4).

6 DISCUSSION

6.1 Mineralogy of the OM regions

The mineralogy of the OM region is complex and rich in carbonates and clay-ammoniated compounds. In addition to the background material, broadly composed of Mg-phyllosilicate, NH_4-phyllosilicates, Ca, Mg-carbonates, and a dark-opaque phase, some spots show the additional presence of sodium carbonates while some others show aliphatic organics, and some others show both (Figs. 4, 5, and 6), as highlighted by the spectra fit analysis (Tables 2, 3, and 4). Moreover, there are some spots that show a very strong and uncommon 3.07-μm band. A more detailed analysis of these spots, using spectral ratios, demonstrates the presence of a band at 2.99–3.0 μm with the organic signatures at 3.4 μm. However, it does not seem to be associated with the presence of NH_4 salts that were indeed identified in Occator bright faculae (De Sanctis et al. 2016; Raponi et al. 2018). The carrier of this band is not yet identified, and we suspect either an additional ammoniated mineral or some amine-bearing compounds. NH-functional groups indeed show absorptions in the range between 2.8 and 3.2 μm that can contribute to the absorption observed.

The observation of ammonium-phyllosilicate material attests to a close relationship between organic and inorganic phases (Ammannito et al. 2016). In fact, the observed correlation between carbonate and aliphatic signatures around Ernutet (Raponi et al. 2017) might indicate that the organic compounds are intimately mixed, and/or chemically bonded with the carbonates. In altered chondrites, a part of the OM is observed as finely interspersed within phyllosilicates and carbonates (Le Guillou et al. 2014; Vinogradoff et al. 2017). Since Ceres has undergone a stronger hydrothermal alteration with more water with respect to chondrites, a large part of the OM might be linked to the inorganic phases in the outer crust of Ceres. The presence of minerals and their transformations during hydrother-

Table 3. Retrieved abundances of spot 5 using different grain size for asphaltite (from Moroz et al. 1998).

Asphaltite (%)	Asphaltite grain size (μm)	Antigorite (%)	NH4-annite (%)	NH4-montmor. (%)	Dolomite (%)	Natrite (%)	Carbon (%)	Grain size (μm)
4.5	0–25	1	0	6	0.5	2.5	85.5	120
5	25–45	2	0	5.5	0.5	3.5	83.5	120
5	45–63	2.5	0	5	0.5	4	83	130
4	63–90	4	2.5	3	1	5	80.5	160
4	90–125	5	4	2	1	5	79	180

Table 4. Retrieved abundances of spot 5 using different end-members for the organic component and dark component.

Asphaltite Shocked (%)	Kerite_2 (%)	Antigorite (%)	NH4-annite (%)	NH4-mont. (%)	Dolomite (%)	Natrite (%)	Carbon (%)	Magnetite (%)	Grain size (μm)
23		1.5	0	9	1	4.5	61	-	115
25.5		3.5	2.5	6.5	1.5	7	-	53	105
	6.5	2	1	7	1.5	2	-	80	125
	5	1	0.5	6	1	1.5	85	-	115

mal alteration in Ceres may have also exerted some influence on the OM evolution (pH variation, fugacity of oxygen, oxidation), but this co-influence remains a subject of investigation.

A mixture with chemical links between organic and inorganic materials could be beneficial for the survival of the OM at the surface of Ceres. Even though the age of the OM material and its exposure time at the surface are not yet determined, irradiation processes (UV, cosmic particles) and space weathering are known to rapidly destroy unprotected organic compounds at the surface of airless bodies (in the span of a few million years) (Clark et al. 2002; Mennella et al. 2003; Pieters & Noble 2016). Phyllosilicates can have a noticeable photoprotective effect on the organic compounds because they have many sites available on the surface and into the interlayer space for molecular absorption (Poch et al. 2015; dos Santos et al. 2016). We may suspect that the excavated material around Ernutet is made of OM, chemically bonded with inorganic phases that would have protected the OM from desorption and destruction by UV irradiation and cosmic rays at the surface.

6.2 Hypothesis for OM origin and evolution

The high-resolution data have shown that the OM is intimately mixed with the mineral phases, which might imply that both phases have evolved together in the early formation of Ceres. Focusing on an endogenous origin of the organic matter in Ceres, we proposed some processes for the formation and evolution of OM, based on Ceres' internal evolution (Castillo-Rogez et al. 2017; McCord & Castillo-Rogez 2017).

The pervasive hydrothermal alteration of Ceres might have created an environment in the interior conducive to producing organic compounds (Holm et al. 2015). Serpentinization processes are likely to have proceeded inside Ceres (Castillo-Rogez et al. 2017), producing serpentine and other hydrated minerals observed at the surface (De Sanctis et al. 2015; Ammannito et al. 2016) and in combination with an another geochemical mechanism, the Fischer–Tropsch-Type process (FTT) (McCollom & Seewald 2007), hydrocarbons can be formed. The FTT process is unique among abiotic processes to provide a source of linear carbon molecules, such as alkanes but also alcohols, and fatty acids (Seewald 2001; McCollom & Seewald 2007; McCollom 2013). At the Ceres scale, FTT reactions may have been very efficient because Ceres is massive enough to have retained H2 from serpentinization for reactions with CO (Castillo-Rogez et al. 2017).

However, the nature of the organic matter formed from serpentinization and FTT processes cannot explain the high abundance of ammonia on Ceres. Due to its correlation with phyllosilicates, it seems that the ammonia was initially present in Ceres' body and so another source of organic matter is required. The diversity and the abundance of organic matter in chondrites, comets, micrometeorites, and interplanetary dust particles indicate that a diverse range of organic materials was present in the protosolar nebula (PSN) before planetary accretion. For the carbonaceous chondrites, it has been suggested that a part of the water was accreted at the same time as some organic matter, enclosed in icy-grains (Le Guillou & Brearley 2014). Considering that the most altered chondrites contain 5 wt per cent of organic matter (Pearson et al. 2006) for about 15 wt per cent of water (Tomeoka & Buseck 1988), the high abundance of water on Ceres (30–35 wt per cent) (Park et al. 2016; Fu et al. 2017) can suggest a higher abundance of OM, around 10–15 wt per cent, accreted in Ceres.

The large amount of ammonia in Ceres' phyllosilicate may come from NH_3-rich ices and/or clathrates (Mousis & Alibert 2005; Shin et al. 2012; Boogert, Gerakines & Whittet 2015) located in the mid-plane of the protoplanetary disk (Caselli & Ceccarelli 2012) that survived transport to feed Ceres' accretion. One can compare the high concentration of ammonia on Ceres with the abundance of ammonia in Jupiter's atmosphere, which is explained (but not entirely understood) by an influx of cold planetesimals (containing ammonia) during Jupiter formation and migration (Atreya et al. 2003). Sources of very diverse and cold materials (formed in the interstellar medium or in the protoplanetary disk) may have drifted inward, closer to the Sun than expected, and Ceres, the largest body of the main belt, could have accreted a higher composition of ammonia and ice (with OM) than other meteorite parent bodies (Mousis & Alibert 2005; McSween et al. 2017). Alternatively, it has been proposed that Ceres could have been formed at great heliocentric distance, in the trans-Neptunian disk, before being implanted in the main belt (McKinnon 2012; De Sanctis et al. 2015), or may have formed closer to Jupiter, and migrated as a result of interactions within the Jupiter system (Kretke et al. 2017). Further observations and studies of other volatile-rich main belt objects are required to understand Ceres' ammonia and organic-rich composition.

In addition, Ceres' materials have undergone hydrothermal alteration processes, as shown by the presence of hydrated minerals, such as abundant phyllosilicates, but also carbonates. The degree of hydrothermal alteration in Ceres was much more severe than in the most altered CC (Brearley 2006; McSween et al. 2017), and must have affected the initial OM. From experimental studies, this hydrothermal alteration seems to be very efficient to rapidly produce a large diversity of molecules, including insoluble materials from simple interstellar and/or protosolar molecules (Kebukawa, Kilcoyne & Cody 2013; Vinogradoff et al. 2018). The high abundance of carbonates in Ceres, for example, might be correlated with the decomposition of molecules and the release of CO_2 during hydrothermal alteration, especially as a correlation has been observed between carbonate and OM abundances around Ernutet (Raponi et al. 2017). In chondrites, it has been observed that an increase of hydrothermal alteration degree increases the abundance of carbonates (Alexander et al. 2015). This is likely due to the loss of their labile fragments into the gas phase (CO_2, CO, CH_4, NH_3) which might have been a more efficient process on Ceres compared to chondrites (McSween et al. 2017). In addition, if FTT products are present in Ceres, they were certainly modified during hydrothermal alteration. In chondrites, linear alcanes are in low abundances because of polymerization, alkylation reactions, and formation of aromatic structures during hydrothermal alteration processes (Elsila et al. 2005; Galvin et al. 2010; Burton et al. 2012).

As the partial differentiation of Ceres proceeded (Park et al. 2016; Prettyman et al. 2017), the most volatile compounds (i.e. organic matter and hydrated minerals) may have been brought together in the outer layer crust. This would have allowed more chemical reactions in the upper layer crust during the pervasive hydrothermal alteration and could explain the presence of organic matter in the upper crust of Ceres.

7 CONCLUDING REMARKS

The high spatial resolution data of VIR analysed here revealed new and interesting findings.

A 2.99–3.0 μm band has been identified in several organic-rich spots. The carrier of this band is not yet identified, and we suspect either an additional ammoniated mineral or some amine-bearing compounds as a component of the OM.

The comparison with laboratory data has shown that the shape and peak positions of the CH aliphatic bands between 3.2 and 3.6 μm are not compatible with a high abundance of oxygen functions (not higher than 20–30 wt per cent) and that the organic oxygen is involved mainly in ketone, ester, ether, or aldehyde functions. Moreover, the non-observation of the CH aromatic band in Ceres spectra do not exclude the presence of aromatic compounds in Ceres OM but instead can provide some clues to the cross-linking level of the carbon structure and/or the abundance of aliphatic carbons. These findings are in agreement with the spectral fit analysis report.

The abundance of the organic matter in the analysed spots has been estimated with a fitting procedure based on Hapke's theory, and we found that such abundance depends on the spectral end members used in the fitting procedure. Several factors influence the estimated abundance, such as the sample grain size and the kind of opaque phases, but their influence seems to be limited to 1–2 per cent on the evaluated amounts. Most important is the organic component considered. The minimum quantity is achieved using spectral end members with a low degree of aromaticity, showing strong aliphatic bands (asphaltite/kerite), while the maximum is obtained when an organic with small aliphatic band is considered (shocked asphaltite). However, considering organic material with a larger degree of aromaticity, such as high kerite/low anthraxolite, the results of the fits are very poor. Thus we can exclude a large abundance of 'aromatic' carbon in the OM of Ceres observed at the surface.

Generally, we found that the estimated abundances of aliphatic carbons in Ceres are larger than the abundance of aliphatic organics normally found in meteorites (Pearson et al. 2006). This may also be seen by the intensity of the CH_2 and CH_3 bands, especially in their antisymmetric stretching modes (Orthous-Daunay et al. 2013); however, remote sensing reflectance spectroscopy cannot be used to assess their quantities.

The mineralogy of the region is revealed to be very complex and rich in carbonates, organic matter, and clay-ammoniated compounds. This heterogeneous mineralogy shows that the evolution of the different components should have been very well mixed in Ceres and especially during the pervasive hydrothermal alteration. Hence, we think that an endogenous source of the OM may be more appropriate, given the Ceres' surface composition, the high retrieved abundances of organics in specific spots, and the observation of some likely extruded materials, even if not directly linked with the region of Ernutet. Indeed, the bright material in the Occator crater, with high Na-carbonates signatures (De Sanctis et al. 2016) and the water ice exposures (Combe et al. 2016; Raponi et al. 2018) and the cryovolcanism (Ruesch et al. 2016) have been explained by activity in Ceres' sub-surface. Thus, it is conceivable that the organic matter localized around the Ernutet crater can also be due to endogenous sources.

Indeed, like other primitive bodies of the main belt, Ceres must have accreted organic matter, ammonia, and carbon present in the protoplanetary formation, to explain at least the high abundance of ammonia into the phyllosilicates. Ceres may have also processed its own organic matter by Fischer–Tropsch-type reactions to produce hydrocarbons from carbon monoxide. Nonetheless, the pervasive hydrothermal alteration on Ceres might have completely modified this accreted or formed organic matter, and some reactions with mineral phases could have occurred, leading to the quite heterogeneous and mixed OM with the mineral phases that we have highlighted here with the VIR high spatial resolution spectra.

ACKNOWLEDGEMENTS

VIR is funded by the Italian Space Agency and was developed under the leadership of INAF-Istituto di Astrofisica e Planetologia Spaziali, Rome, Italy. The instrument was built by Selex-Galileo, Florence, Italy. The authors acknowledge M. Ferrari for his help with the laboratory measurements. The authors acknowledge the support of the Dawn Science, Instrument, and Operations Teams. This work was supported by the Italian Space Agency and NASA. A portion of this work was performed at the Jet Propulsion Laboratory under contract with NASA. This research utilizes spectra of the NASA RELAB facility at Brown University. We thank Dr. L. Moroz for providing us the spectra of solid bitumen used here for the fit.

REFERENCES

Alexander C. M. O., Bowden R., Fogel M. L., Howard K. T., 2015, Meteorit Planet Sci, 50, 810

Alexander C. M. O., Fogel M., Yabuta H., Cody G. D., 2007, Geochim. Cosmochimi. Acta, 71, 4380

Ammannito E. et al., 2016, Science, 353, 1006

Atreya S. K., Mahaffy P. R., Niemann H. B., Wong M. H., Owen T. C., 2003, Planet. Space Sci.., 51, 105
Bernard S., Horsfield B., Schulz H.-M., Wirth R., Schreiber A., Sherwood N., 2012, Mari. Pet. Geol., 31, 70
Bishop J. L., Banin A., Mancinelli R. L., Klovstad M. R., 2002, Planet. Space Sci., 50, 11
Boogert A., Gerakines P., Whittet D., 2015, Annu. Rev. Astron. Astrophys., 53, 541
Brearley A. J., 2006, Lauretta D. S., McSween H. Y., Jr., The Action of Water, in: Meteorites and the Early Solar System II. Univ. Arizona Press, p. 584
Bree A., Zwarich R., 1969, J. Chem. Phys., 51, 912
Burton A. S., Stern J. C., Elsila J. E., Glavin D. P., Dworkin J. P., 2012, Chem. Soc. Rev., 41, 5459
Capaccioni F. et al., 2015, Science, 347, aaa0628
Carrozzo F. G., Raponi A., De Sanctis M. C., Ammannito E., Giardino M., D'Aversa E., Fonte S., Tosi F., 2016, Rev. Sci. Instrum., 87, 124501
Carrozzo F. G. et al., 2018, Sci. Adv., 4, 3
Caselli P., Ceccarelli C., 2012, Astron Astrophys Rev, 20, 56
Castillo-Rogez J. C., Neveu M., McSween H. Y., Fu R. R., Toplis M., Prettyman T., 2017, Meteoritics & Planetary Science forthcoming
Ciarniello M. et al., 2011, Icarus, 214, 541
Clark B. E., Hapke B., Pieters C., Britt D., 2002, Asteroid Space Weathering and Regolith Evolution, in: Asteroids III. p. 585
Cloutis E. A., 2003, Fuel, 82, 2239
Coates J., 2006, Interpretation of Infrared Spectra, A Practical Approach, in: Encyclopedia of Analytical Chemistry. John Wiley & Sons, Ltd
Cody G. D., Alexander C. M. O., Tera F., 2002, Geochimica et Cosmochimica Acta, 66, 1851
Cody G. D., Alexander C. M. O'.D., 2005, Geochimica et Cosmochimica Acta, 69, 1085
Combe J.-Ph. et al., 2016, Science, 353
Curiale J. A., 1986, Organic Geochemistry, 10, 559
Danger G., Rimola A., Mrad N. A., Duvernay F., Roussin G., Theule P., Chiavassa T., 2014, Physical Chemistry Chemical Physics, 16, 3360
Dartois E. et al., 2007, IRAS 08572+3915: constraining the aromatic versus aliphatic content
De Angelis S. et al., 2015, Review of Scientific Instruments, 86, 093101
Dela Rosa L., Pruski M., Lang D., Gerstein B., Solomon P., 1992, Energy Fuels, 6, 460
De Sanctis M. C. et al., 2011, Space Science Reviews, 163, 329
De Sanctis M. C. et al., 2015, Nature, 528, 241
De Sanctis M. C. et al., 2016, Nature, 528, 241
De Sanctis M. C. et al., 2017, Science, 355, 719
De Sanctis M. C. et al., 2018, Meteoritics & Planetary Science, 53, 1844
dos Santos R., Patel M., Cuadros J., Martins Z., 2016, Icarus, 277, 342
Ehlmann B. L., Hodyss R., Ammannito E., Rossman G. R., De Sanctis M. C., Raymond C. A., 2018, Meteoritics & Planetary Science, 53, 1884
Elsila J. E., de Leon N. P., Buseck P. R., Zare R. N., 2005, Geochimica et Cosmochimica Acta, 69, 1349
Fu R. R. et al., 2017, Earth and Planetary Science Letters, 476, 153
Glavin D. P., Callahan M. P., Dworkin J. P., Elsila J. E., 2010, Meteoritics & Planetary Science, 45, 1948
Hapke B., 2012, Theory of reflectance and emittance spectroscopy. Cambsridge University Press
Holm N. G., Oze C., Mousis O., Waite J. H., Guilbert-Lepoutre A., 2015, Astrobiology, 15, 587
Kebukawa Y., Kilcoyne A. L. D., Cody G. D., 2013, ApJ, 771, 19
King T. V., Clark R. N., Calvin W. M., Sherman D. M., Brown R. H., 1992, Science, 255, 1551
Kretke K. A., Bottke W., Kring D. A., Levison H. F., 2017, Effect of Giant Planet Formation on the Compositional Mixture of the Asteroid Belt. Presented at the AAS/Division of Dynamical Astronomy Meeting, p. 103.02
Le Guillou C., Bernard S., Brearley A. J., Remusat L., 2014, Geochimica et Cosmochimica acta , 131, 368
Le guilou C., Breale A., 2014, Geochimica et cosmochimica Acta, 131, 344
Lis G. P., Mastalerz M., Schimmelmann A., Lewan M. D., Stankiewicz B. A., 2005, Organic geochemistry, 36, 1533
McCollom T. M., 2013, Reviews in Mineralogy and Geochemistry, 75, 467
McCollom T. M., Seewald J. S., 2007, Chem. Rev., 107, 382
McCord T. B., Castillo-Rogez J., 2018, Meteoritics & Planetary Science, 53, 1778
McKinnon W. B., 2012, Where Did Ceres Accrete? Presented at the Asteroids, Comets, Meteors 2012. Lunar and Planetary Institute LPI, Houston, USA, p. 6475
McSween H. Y. et al., 2017, Meteorit. Planet Sci., 53, 1793
Mennella V., Baratta G. A., Esposito A., Ferini G., Pendleton Y. J., 2003, ApJ, 587, 727
Moroz L. V., Arnold G., Korochantsev A. V., Wäsch R., 1998, Icarus, 134, 253
Mousis O., Alibert Y., 2005, MNRAS, 358, 188
NIST Mass Spec Data Center, 2018, in Linstrom P. J., Mallard W. G.eds, 'Infrared Spectra' in the WebBook of Chemistry NIST, Data base N 69. National Institute of Standards and Technology, Gaithersburg MD
Orthous-Daunay F.-R., Quirico E., Beck P., Brissaud O., Dartois E., Pino T., Schmitt B., 2013, Icarus, 223, 534
Park R. S. et al., 2016, Nature, 537, 515
Pasckert J. H. et al., 2017, Icarus, in press
Pearson V. K., Sephton M. A., Franchi I. A., Gibson J. M., Gilmour I., 2006, Meteorit. Planet. Sci., 41, 1899
Pieters C. M., Noble S. K., 2016, J. Geophys. Res. Planets, 121, 1865
Pieters C. M. A. et al., 2017, Meteorit. Planet. Sci., 53, 1983
Poch O., Jaber M., Stalport F., Nowak S., Georgelin T., Lambert J.-F., Szopa C., Coll P., 2015, Astrobiology, 15, 221
Prettyman T. H. et al., 2017, Science, 355, 55
Quirico E. et al., 2016, Icarus, 272, 32
Raponi A.. et al., 2017, Icarus, in press
Raponi A. et al., 2018, Icarus, in press
RELAB [WWW Document], n.d. URL http://www.planetary.brown.edu/relab/
Ruesch O. et al., 2016, Science, 353, 1005
Russell C. T. et al., 2016, Science, 353, 1008
Schutte W. A., Allamandola L. J., Sandford S. A., 1993, Icarus, 104, 118
Seewald J. S., 2001, Geochimica et Cosmochimica Acta, 65, 1641
Shin K., Kumar R., Udachin K. A., Alavi S., Ripmeester J. A., 2012, Proc. Natl. Acad. Sci. U. S. A., 109, 14785
Tomeoka K., Buseck P. R., 1988, Geochim. Cosmochim. Acta, 52, 1627
Vinogradoff V., Bernard S., Le Guillou C., Remusat L., 2018, Icarus, 305, 358
Vinogradoff V., Le guillou C., Bernard S., Binet L., Cartigny P., Brealey A. J., Remusat L., 2017, Geochimica et Cosmochimica acta, 212, 234
Zubko V. G. et al., 1996, MNRAS, 282, 1321

This paper has been typeset from a TEX/LATEX file prepared by the author.